# A secreted protease-like protein in *Zymoseptoria tritici* is responsible for avirulence on *Stb9* resistance gene in wheat

Reda AMEZROU[1], Colette AUDÉON[1], Jérôme COMPAIN[2], Sandrine GÉLISSE[1], Aurélie DUCASSE[1], Cyrille SAINTENAC[3], Nicolas LAPALU[1,2], Clémentine LOUET[1], Simon ORFORD[4], Daniel CROLL[5], Joëlle AMSELEM[2], Sabine FILLINGER[1], Thierry C MARCEL[1*]

[1] Université Paris-Saclay, INRAE, UR BIOGER, 91120 Palaiseau, France.
[2] Université Paris-Saclay, INRAE, UR URGI, 78026 Versailles, France.
[3] UCA, INRAE, GDEC, 63000 Clermont-Ferrand, France.
[4] Crop Genetics, John Innes Centre, Norwich NR4 7UH, UK.
[5] University of Neuchâtel, Laboratory of Evolutionary Genetics, 2000 Neuchâtel, Switzerland.

[*] Corresponding authors: thierry.marcel@inrae.fr; reda.amezrou@inrae.fr

**Running title:** The avirulence factor *AvrStb9* from *Zymoseptoria tritici*

**Key words:** Avirulence, Gene-for-gene interaction, Protease, GWAS, Wheat, *Zymoseptoria tritici*

## Abstract

*Zymoseptoria tritici* is the fungal pathogen responsible for Septoria tritici blotch on wheat. Disease outcome in this pathosystem is partly determined by isolate-specific resistance, where wheat resistance genes recognize specific fungal factors triggering an immune response. Despite the large number of known wheat resistance genes, fungal molecular determinants involved in such cultivar-specific resistance remain largely unknown. We identified the avirulence factor *AvrStb9* using association mapping and functional validation approaches. Pathotyping *AvrStb9* transgenic strains on *Stb9* cultivars, near isogenic lines and wheat mapping populations, showed that *AvrStb9* interacts with *Stb9* resistance gene, triggering an immune response. *AvrStb9* encodes an unusually large avirulence gene with a predicted secretion signal and a protease domain. It belongs to a S41 protease family conserved across different filamentous fungi in the Ascomycota class and may constitute a core effector. *AvrStb9* is also conserved among a global *Z. tritici* population and carries multiple amino acid substitutions caused by strong positive diversifying selection. These results demonstrate the contribution of an 'atypical' conserved effector protein to fungal avirulence and the role of sequence diversification in the escape of host recognition, adding to our understanding of host-pathogen interactions and the evolutionary processes underlying pathogen adaptation.

## Author Summary

Fungal avirulence (*Avr*) genes are involved in gene-for-gene relationships with host resistance genes. *Avr* genes may at the same time target host defenses to allow infection and be recognized by a host resistance gene triggering a defense response. The fungus *Zymoseptoria tritici* causes Septoria tritici blotch, a major disease of wheat worldwide. *Z. tritici* populations rapidly adapt to selection pressures such as host resistance, leading to resistance breakdown. We report the identification of the avirulence gene *AvrStb9* based on genetic mapping, sequence polymorphisms and allele swapping. *AvrStb9* is involved in the interaction with *Stb9* resistance gene following the gene-for-gene model, and its recognition hinders disease symptoms in hosts carrying the corresponding resistance gene. Unlike other known *Z. tritici Avr* effectors, *AvrStb9* encodes for an unusually large Avr protein with a predicted protease S41 domain conserved among diverse ascomycete lineages. We also highlight several gene mutations likely involved in escaping *Stb9*-mediated recognition.

## Introduction

Filamentous fungal pathogens are responsible for some of the most damaging crop diseases [1]. Their ability to cause disease is facilitated by fungal proteins called effectors, which are delivered into the plant apoplast or cytoplasm during the infection process [2,3]. Effectors play critical roles in the infection by manipulating plant immune system and other cellular functions. To counteract fungal infections, plants have evolved efficient defense systems relying on the recognition of different fungal factors [4]. The first type of defense involves plant receptors recognizing generic fungal molecules, called pathogen-associated molecular patterns (PAMPs). This PAMP-triggered immunity (PTI) provides basal defense against non-adapted pathogens. The second type of defense is activated with the recognition of fungal effectors by plant receptors, defined as resistance (*R*) genes. Effector-triggered immunity (ETI) induces a specific and strong immune response thought to limit the infection [4]. This interaction typically follows the gene-for-gene model, where host *R* gene products recognize pathogen effectors, which are then called avirulence (*Avr*) genes [5]. However, ETI exerts a strong evolutionary pressure on pathogen populations leading to the selection of virulent isolates overcoming host immune response [2]. Most of these virulent isolates displayed mutations in the avirulence gene leading to variant proteins not recognized by the corresponding R protein [6]. These observations emphasize the importance of pathogen *Avr* genes surveillance and the adequate spatiotemporal deployment of *R* genes in the field.

Most of the characterized fungal effector genes encode secreted proteins and lack sequence similarities with other species [7,8]. However, the analysis of protein structures suggests that fungal effectors can be grouped in structurally related families [9-11]. In addition, a number of effectors in plant pathogenic fungi are predicted to encode proteins that share similarities with known enzymes or enzyme inhibitors (reviewed in [8]), *e.g.* some *Avr* genes from *Cladosporium fulvum* (*Avr2* and *Avr4*), *Magnaporthe oryzae* (*Avr-Pita*) or *Melampsora lini* (*AvrM14*). However, only few have been reported to be involved in fungal

avirulence, and their identification will broaden our knowledge on the complex molecular cross-talk between plants and pathogens.

*Zymoseptoria tritici* is an ascomycete fungal pathogen that causes the major wheat foliar disease Septoria tritici blotch (STB). *Z. tritici* is apoplastic with a biphasic infection process [12]. After penetration into wheat leaves through stomata, the fungus colonizes the apoplast for 8-11 days while the host remains symptomless [13]. This long asymptomatic phase is followed by a rapid onset of necrotic symptoms, associated with the development of fungal asexual fruiting bodies called pycnidia, which contain the pycnidiospores that further spread the disease [14]. STB is currently the economically most important wheat disease in Europe and is mainly controlled using fungicides and genetic resistances [12,15]. However, this disease remains a problem due to the ability of fungal populations to overcome control measures (*i.e.*, fungicide resistance, host resistance breakdown) and adapt to climate changes [15]. Despite its economic importance, the molecular basis of *Z. tritici* avirulence remains largely unknown. Only two avirulence genes have been characterized so far, *AvrStb6*, recognized by the resistance protein *Stb6* leading to a strong immune response; and *Avr3D1* which is thought to trigger quantitative resistance in cultivars carrying *Stb7* resistance gene [16,17,18]. Both genes encode small secreted proteins located in highly plastic genomic regions rich in transposable elements thought to favor their rapid diversification [16,18]. In addition to *Stb6* and *Stb7*, 21 major isolate-specific STB resistance genes have been mapped in wheat, but their corresponding avirulence genes remain unknown [19,20,21].

Here, we aimed to broaden our understanding of avirulence in fungal pathogens, the mechanisms underlying gene-for-gene interactions in the *Z. tritici*–wheat pathosystem and the evolutionary processes related to the escape of host recognition. We first showed that a large protein encoding a predicted secreted protease, *AvrStb9*, is responsible for avirulence in a subset of fungal strains. We demonstrated that recognition of *AvrStb9* by hosts carrying *Stb9* resistance gene triggers an immune response following the gene-for-gene model. We next showed that *AvrStb9* belongs to a family of proteins with a predicted protease S41 domain conserved across diverse ascomycete lineages and that mutations in *AvrStb9*, including some in the predicted protease domain, led to variants escaping *Stb9*-mediated recognition.

## Results

### Mapping of a candidate gene conferring avirulence on the cultivar 'Soissons'.

'Soissons' is a French bread wheat variety, developed by Florimond Desprez and released in 1987, which represented 10 to 40% of the French wheat acreage between 1991 and 2002. 'Soissons' is moderately susceptible to STB [22] but it has been postulated to carry the resistance gene *Stb9* based on screening with differentially virulent isolates. Infection assays of the fungal population showed that

107 ~12% of the French isolates are avirulent on cultivar 'Soissons' (Fig. S1). We conducted GWAS to
108 identify the *Avr* gene interacting with the resistance in 'Soissons'.

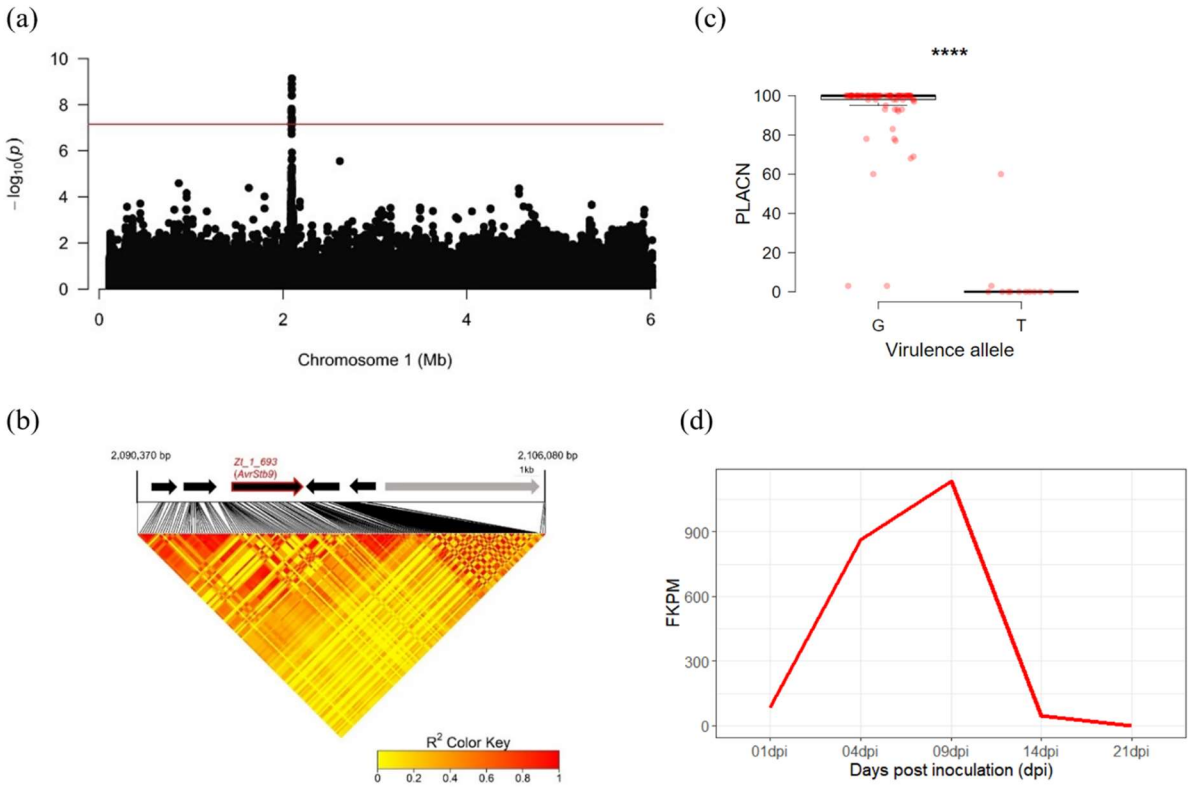


109

110 **Figure 1.** GWAS identifies a candidate gene controlling avirulence on the cultivar 'Soissons'. (a) Manhattan plot
111 representing the association of multiple SNPs with the percentage of leaf area covered by necrosis (PLACN) on
112 cultivar 'Soissons'. The X and Y axes indicate positions on chromosome 1 and −log10 (*p*-value) for associations,
113 while the red line represents the Bonferroni threshold (α=0.05). (b) Top: Gene annotations (black arrows) and
114 transposable elements (grey arrow) on the reference genome IPO323. The candidate gene is highlighted in red.
115 Bottom: Pairwise linkage disequilibrium plot around the lead significant SNP. The association peak is associated
116 with several polymorphisms in the gene *Zt_1_693*. (c) The difference in PLACN of isolates carrying the virulent
117 and avirulent alleles (based on the lead SNP). Significance difference from the mean was computed using a two-
118 sided Mann-Whitney test (****, $p<0.0001$). (d) Gene expression profile of *Zt_1_693* measured as fragments per
119 kilobase of exon per million mapped fragments (FPKM) throughout the time course of *Z. tritici* infection on a
120 susceptible wheat cultivar [23].

121 A total of 103 *Z. tritici* strains were re-sequenced, generating 718,810 SNPs passing quality filters. Using
122 full SNP data, we investigated the population structure and kinship and found very little genetic
123 substructure and relatedness in the fungal population (Fig. S2a,b). For instance, the first three PCs
124 accounted for only 3.11% of the total genetic variation. Using a linear mixed model to associate genetic
125 variations with pycnidia (PLACP) and necrosis (PLACN) variations on 'Soissons', we identified a
126 cluster of 26 SNPs on chromosome 1 from 2,092,563 bp to 2,096,143 bp, significantly associated with
127 PLACN at the Bonferroni threshold (Fig. 1a). The same SNP cluster was also associated with variation

128 in PLACP but failed to reach the genome-wide significance (Fig. S3). We also detected a significant
129 association with PLACN variations ($p$=3.801e-8; position 2,451,010 bp) on a segment of chromosome
130 7. However, the region falls in a broad section of the chromosome without any *in planta* expressed genes
131 [23]. The significant SNPs on chromosome 1 mapped to a region containing two predicted genes,
132 *Zt_1_692* and *Zt_1_693*. The lead SNP ($p$=7.31e-10; position 2,095,552 bp) mapped to the fourth exon
133 of *Zt_1_693*, but was in strong linkage disequilibrium with other variants spanned across the two
134 predicted genes (Fig. 1b). *Zt_1_692* is not expressed *in planta* so we were unable to use RNA-seq data
135 to evaluate the quality of the gene annotation and blastp searches yielded only weak hits. Without any
136 corroborating evidence for a biological role, we concluded that *Zt_1_692* is likely a pseudogene or an
137 annotation error. In contrast, *Zt_1_693* is highly expressed *in planta* (Fig. S4), with a peak expression
138 at 9 days post infection coinciding with the switch from asymptomatic to necrotrophic phase (Fig. 1d).
139 Further, allele analyses of the lead SNP clearly discriminated between avirulent and virulent phenotypes
140 (Fig. 1c). Taken together, we considered *Zt_1_693* as the best candidate gene to explain avirulence on
141 the wheat cultivar 'Soissons'.

142 ***Zt_1_693* is involved in a gene-for-gene relationship with *Stb9* resistance gene.**

143 To determine whether *Zt_1_693* is an avirulence factor recognized by an *R* gene in the cultivar
144 'Soissons', we sought to generate *Zt_1_693* deletion mutants (KO) in the virulent strain IPO323 and
145 four different avirulent strains by targeted gene replacement. We also switched alleles between avirulent
146 (IPO09395) and virulent (IPO323) strains using targeted gene replacement. However, we could not
147 obtain any deletion mutant neither in IPO323 (144 transformants tested), nor in the avirulent strains
148 IPO09593, IPO09359 and IPO09139 (n=95). Only a single deletion mutant was obtained in strain
149 SYN32 out of 32 transformants, producing small colonies and weak symptoms on the susceptible
150 cultivar 'Taichung-29' (Table S1). This suggests that *Zt_1_693* could be essential for *Z. tritici* growth,
151 and pathogenicity. Nevertheless, using allele swapping we were able to generate mutants expressing the
152 virulent and avirulent versions of *Zt_1_693* in IPO323 genetic background, and performed infection
153 assays on cultivars 'Soissons', 'Courtot' which carries the *Stb9* gene and a 'Courtot' near isogenic line
154 lacking *Stb9*.

155 IPO323 gene replacement transformants carrying the avirulent allele (n=6) from IPO09593 (referred to
156 as *Avrstb9*) were avirulent on 'Soissons' and 'Courtot', but not on 'Courtot' lacking *Stb9* (Fig. 2a).
157 Inversely, gene replacement transformants with the virulent allele (referred to as *avrstb9*) from IPO323
158 (n=2) resulted in virulence on all tested cultivars, with PLACP values at 26 dpi ranging from 32 to 100%
159 (Fig. 2a). Interestingly, Sanger sequencing of IPO323$_{Avrstb9}$ transformants revealed that four strains were
160 chimeric with the avirulent allele not being introduced in full length, retaining some polymorphisms of
161 the virulent haplotype between residues 276 and 628. All four chimeric strains were virulent on *Stb9*-
162 containing cultivars, highlighting the importance of these polymorphisms in virulence (Table 1; Table

S1; Fig. S5). The fact that all IPO323 mutants carrying the complete *AvrStb9* allele were unable to infect *Stb9*-containing cultivars, while mutants expressing the *avrStb9* allele produced symptoms on all three cultivars, suggest that *Zt_1_693* encodes the avirulence factor *AvrStb9*, which triggers complete resistance in cultivars carrying the cognate resistance gene.

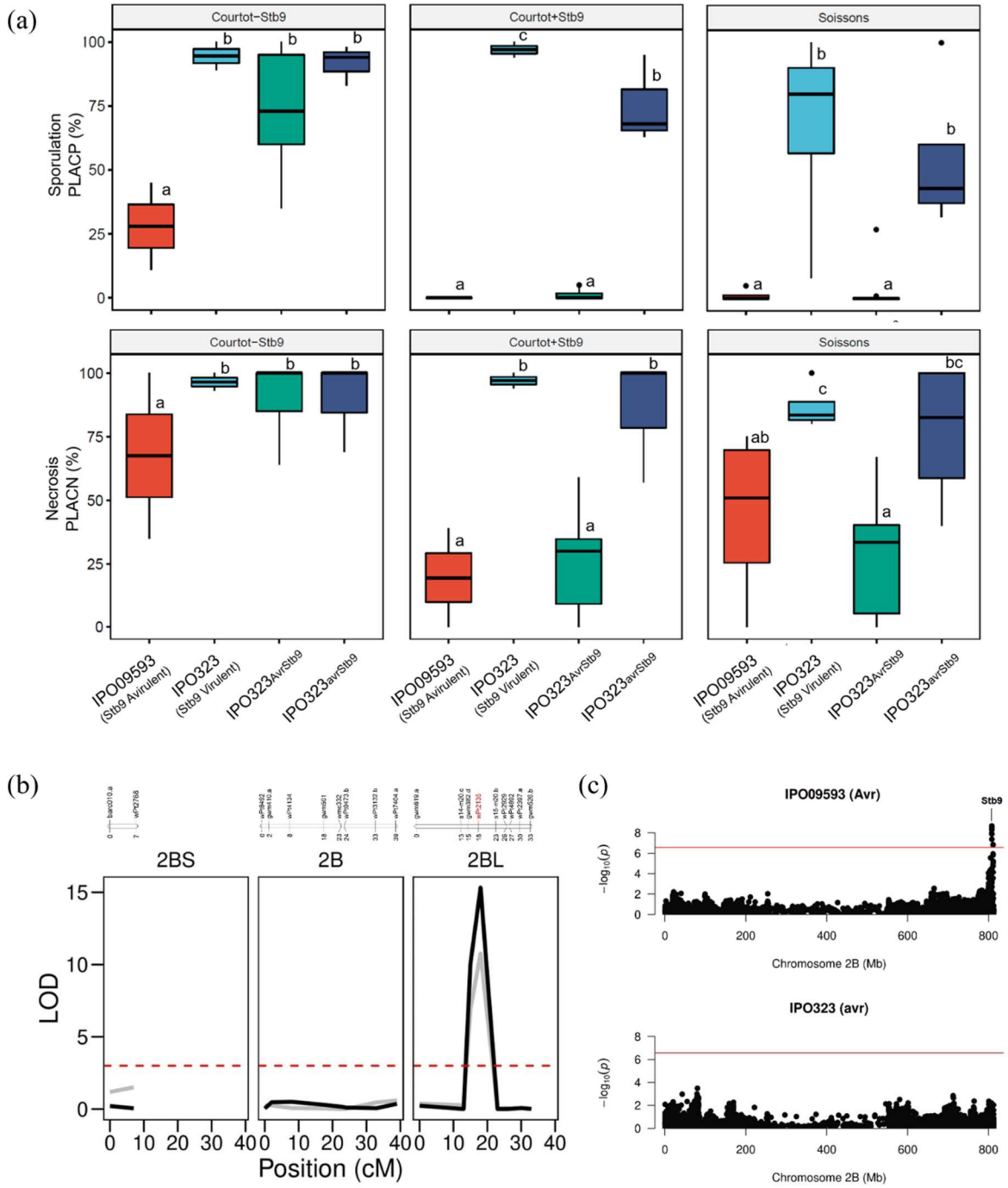


**Figure 2.** *Zt_1_693* encodes for the avirulence gene *AvrStb9* and triggers *Stb9* resistance. (a) Percentage of leaf area covered by pycnidia (PLACP) and percentage of leaf area covered by necrosis (PLACN) at 26 dpi measured after inoculation with the avirulent isolate IPO09593, the virulent isolate IPO323 and IPO323 transformants carrying the avirulent allele (IPO323$_{Avrstb9}$) or the virulent allele (IPO323$_{avrstb9}$) on cultivars 'Courtot' (*Stb9*), a 'Courtot' mutant lacking *Stb9* and 'Soissons' (details on the phenotype of each mutant is provided in Fig. S5;

173 Table S1). Letter above the boxplots represent statistical groups based on a post-hoc Tukey's HSD test (α = 0.05)
174 performed independently for each wheat background. (b) Genetic mapping of *Stb9* resistance gene using linkage
175 mapping. Top panel: Linkage map and marker position in cM. Bottom panel: Logarithm of odds (LOD) score plot
176 of the QTL analysis (Relative AUDPC for sporulation and necrosis in black and grey, respectively) possibly
177 containing the *Stb9* locus mapped to the long arm of the chromosome 2B. The horizontal dashed line indicates a
178 suggestive linkage threshold (LOD = 3). The position of the marker in the QTL peak is highlighted in red. (c)
179 Manhattan plots representing association mapping results of relative AUDPC sporulation of the avirulent (top) and
180 virulent (bottom) isolates in the bread wheat panel. Multiple SNPs in the telomeric region of chromosome 2B
181 associated with the avirulent isolate are located in the *Stb9* genomic region.

182 To further validate the *AvrStb9-Stb9* gene-for-gene relationship, we performed two independent genetic
183 analyses using a bi-parental mapping population and a panel of wheat varieties. The isolate-specific
184 resistance to IPO09593 (*AvrStb9*) was mapped by a QTL analysis on Beaver/Soissons recombinant
185 double haploid progenies. A single major resistance QTL was detected on the long arm of the wheat
186 chromosome 2B, likely corresponding to the *Stb9* locus [24]. This QTL had a log-likelihood (LOD) of
187 10.77 and 15.33 for the RAUDPC of necrosis and sporulation, respectively (Fig. 2b). As expected, the
188 resistance allele originated from 'Soissons' suggesting that the cultivar indeed carries the *Stb9*
189 resistance. We confirmed this interaction by performing a GWAS analysis on a wheat panel phenotyped
190 using the virulent and avirulent strains. Association mapping results revealed a strong signal associated
191 with RAUDPCs for the avirulent strain IPO09593 (eight SNPs above the Bonferroni-corrected cutoff)
192 in the telomeric region of chromosome 2B, but not with the virulent strain IPO323 (Fig. 2c). This
193 confirms that IPO09593 triggers a strong resistance from varieties carrying a resistance QTL in the
194 vicinity of the *Stb9* gene. Additional details on *Stb9*-associated SNPs are provided in the supplemental
195 Table S2. Finally, based on the lead SNP (AX-89505650; position 808,036,267 bp on chromosome 2B),
196 phenotypic and allele analyses showed that ca. 8.2% of the French varieties likely carry *Stb9* (Fig. S6).

197 Altogether, our combined functional and genetic analyses demonstrate that *Zt_1_693* is the avirulence
198 gene *AvrStb9* and is involved in a gene-for-gene relationship with *Stb9* resistance in wheat.

199 ***AvrStb9* encodes a secreted protein with a conserved protease domain shared among diverse**
200 **ascomycete lineages.**

201 Unlike other known fungal effectors, *AvrStb9* encodes a large protein and shares sequence similarities
202 with different fungal species. The re-annotated *AvrStb9* gene model has five introns and encodes a 727
203 amino acid long protein with eight cysteine residues (Fig. 3a; 3b). This protein has a predicted signal
204 peptide sequence of 18 amino acids at its N-terminus and two serine-protease domains (C-terminal
205 processing peptidase S41 family; positions 70-726; Fig. 3b) according to InterProScan (Panther entry
206 PTHR-37049, e-value: 2.7 e-64). HHpred searches in protein structure databases identified the secreted

207 **Table 1.** Polymorphisms in AvrStb9 protein sequences between the wild type and transgenic mutant strains. Difference in amino acid residues between the
208 virulent (avrstb9) and avirulent (Avrstb9) phenotypes are highlighted in orange while residues potentially involved in virulence are highlighted in red.

| **Strain** | **Mutant ID** | **Codon position / Amino acid residue** | | | | | | | | | | | | | **Phenotype (on *Stb9*)** |
|---|---|---|---|---|---|---|---|---|---|---|---|---|---|---|---|
| | | **58** | **66-71** | **73** | **188** | **276** | **349** | **370** | **431** | **473** | **512** | **525** | **565** | **628** | |
| **Wild-type strains** | | | | | | | | | | | | | | | |
| IPO323 (avrstb9) | - | R | PCNSTI | N | Y | T | A | T | A | F | S | S | D | L | Virulent |
| IPO09593 (Avrstb9) | - | Q | Δ | D | V | N | V | N | D | Y | T | F | N | Y | Avirulent |
| **IPO323 Avrstb9 transformants** | | | | | | | | | | | | | | | |
| IPO323$_{Avrstb9}$ hph#5 | E | Q | Δ | D | V | N | V | N | D | Y | T | F | N | Y | Avirulent |
| IPO323$_{Avrstb9}$ hph#6 | F | Q | Δ | D | V | N | V | N | D | Y | T | F | N | Y | Avirulent |
| IPO323$_{Avrstb9}$ hph#9 | H | Q | Δ | D | V | N | V | N | D | Y | T | F | N | Y | Avirulent |
| IPO323$_{Avrstb9}$ hph#12 | K | Q | Δ | D | V | N | V | N | D | Y | T | F | N | Y | Avirulent |
| IPO323$_{Avrstb9}$ hph#14 | L | Q | Δ | D | V | N | V | N | D | Y | T | F | N | Y | Avirulent |
| IPO323$_{Avrstb9}$ hph#18 | N | Q | Δ | D | V | N | V | N | D | Y | T | F | N | Y | Avirulent |
| **IPO323 Avrstb9 chimeric transformants** | | | | | | | | | | | | | | | |
| IPO323$_{Avrstb9}$ hph#3 | I | Q | Δ | D | V | T | A | T | A | F | S | S | D | L | Virulent |
| IPO323$_{Avrstb9}$ hph#11 | J | Q | Δ | D | Y | T | A | T | A | F | S | S | D | L | Virulent |
| IPO323$_{Avrstb9}$ hph#7 | G | Q | Δ | D | Y | T | A | T | A | F | S | S | D | L | Virulent |
| IPO323$_{Avrstb9}$ hph#17 | M | Q | Δ | D | V | N | A | T | A | F | S | S | D | L | Virulent |
| **IPO323 avrstb9 transformants** | | | | | | | | | | | | | | | |
| IPO323$_{avrstb9}$ hph#3 | O | R | PCNSTI | N | Y | T | A | T | A | F | S | S | D | L | Virulent |
| IPO323$_{avrstb9}$ hph#4 | P | R | PCNSTI | N | Y | T | A | T | A | F | S | S | D | L | Virulent |
| | | | | | | | | | | | | | | | |
| Percentage of virulent isolates in the fungal population | | 87.5 | 98.86 | 86.63 | 98.86 | 98.86 | 54.54 | 88.63 | **98.86** | **98.86** | 89.77 | **98.86** | **98.86** | **95.54** | |
| Probability of dN/dS>1 | | 0.97 | - | 0.99 | 0.99 | 0.58 | 0.54 | 0.59 | 0.93 | 0.60 | **0.99** | **1.00** | 0.65 | **1.00** | |

209

protease CPAF as the strongest hit (e-value of 1.5e-27), which is involved in pathogenesis of the human pathogenic bacterium *Chlamydia trachomatis* [25]. The predicted protein structure of AvrStb9 was used to search for structural similarity in PDB, which identified the same protease CPAF with highest similarity to AvrStb9 (DALI Z-score 16.5) (Table S3). Mature CPAF is a homodimer comprised of two distinct subunits, chains A and B [25]. The pairwise structure alignment of AvrStb9 with both chains of CPAF confirms the structural similarities with a TM-score of 0.56 (Table S4).

To investigate whether *AvrStb9* originated before or after *Z. tritici* speciation, we used blastp searches against *Z. tritci* reference genome IPO323 and closely-related species from the *Zymoseptoria* family. We identified *AvrStb9* and its paralogs from IPO323 and all its closest relatives *Z. pseudotritici, Z. ardabiliae* and *Z. brevis* (Fig. S7a). Interestingly, most of these proteins had a predicted signal peptide, and they all displayed a C-terminal processing peptidase S41 domain. Using IPO323 *in planta* gene expression, we found that three out of the five paralogs (*Zt_4_489, Zt_10_226, Zt_11_236*) had an expression profile comparable to *AvrStb9* (Fig. S7b). According to these expression patterns, these genes could potentially play a role in infection.

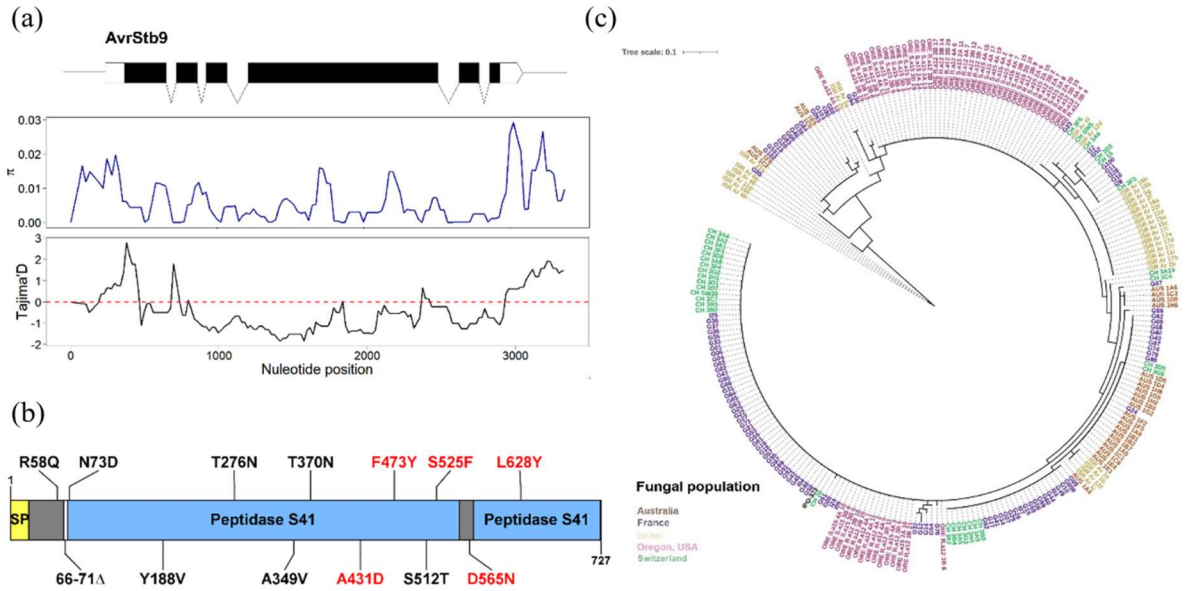


**Figure 3.** *AvrStb9* diversity and phylogeny in the global *Z. tritici* population. (a) The top panel shows the *AvrStb9* gene structure. Middle and low panels are sliding window analyses for nucleotide diversity (π) and Tajima's D across the *AvrStb9* locus, respectively, with a window size of 200 bp and a step size of 20 bp. The plots show a reduced nucleotide diversity and a drop in Tajima's D values, likely corresponding to a selective sweep spanning the region. (b) Schematic diagram of *AvrStb9* protein sequence with an annotation of amino acid substitutions between virulent and avirulent alleles. Substitutions potentially involved in virulence are highlighted in red. SP=Signal peptide. (c) A phylogenetic tree of *AvrStb9* protein sequence generated from a global *Z. tritici* population and the reference isolate IPO323.

Using OrthoMCL, we identified 122 putative *AvrStb9* orthologs/paralogs with an average identity of 33.6% and an average e-value of 8e-73 (Table S5). *AvrStb9* orthologs/paralogs are found in a broad

range of ascomycete lineages belonging to Eurotiomycetes, Leotiomycetes, Sordariomycetes, Orbiliomycetes and Dothideomycetes (Fig. 4; Table S5). Most of fungal species (48 out of 65 species) identified from the orthogroup are pathogenic, indicating that the well conserved *AvrStb9* orthologs/paralogs may be involved in host interaction processes. Interestingly, ~87% of these proteases possess a predicted signal peptide.

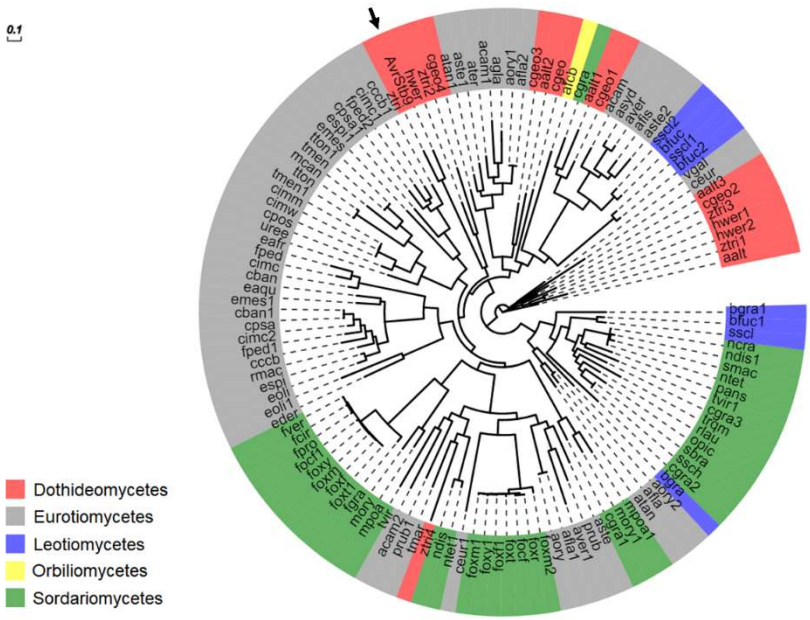


**Figure 4.** Phylogenetic tree of selected *AvrStb9* orthologs/paralogs belonging to five distinct classes of Ascomycota lineages. Leaf labels are color-coded according to class and represent abbreviated names of the fungal species (Table S5). *AvrStb9* is indicated with a black arrow.

## Diversification of *AvrStb9* leads to evasion of host recognition

Non-synonymous substitutions in avirulence gene sequences often mediate the evasion of host recognition. Analysis of sequence polymorphisms between the avirulent and virulent strains revealed a 6 amino acid deletion and 12 non-synonymous substitutions (Table 1; Fig. 3b). We crossed this data with the fungal population phenotypes and identified eight mutations potentially involved in host evasion for which more than ~94% of strains carrying the mutation were virulent on *Stb9* cultivars (Table 1). Five of these mutations fall into the virulence-domain cited above, namely A431, F473, S525, D565, L628. All of these mutations except D565 are located in one of the two putative protease domains (Fig. 3b), with F473, S525 and L628 being relatively conserved residues among proteins belonging to the CPAF structural family (in 34-57% of the analyzed proteins respectively).-The visualization of these five residues on the predicted protein structure of avrStb9 revealed their physical proximity (Fig. 5b). The predicted structures of AvrStb9 and avrStb9 aligned with 94% sequence identity (TM-score of 0.94) (Fig. 5a; Table S4), not indicating any important structural changes between both protein variants. Comparing the physical distances between the five residues on AvrStb9 and avrStb9 predicted structures

identified the residue S525 (*vs.* F525) as being much more distant (10-27%) from the other four residues in the virulent avrStb9 compared to the avirulent AvrStb9 predicted structure. In addition, the F to S modification at position 525 replaces a polar residue by a hydrophobic one. This may indicate the importance of the 525 residue in escaping recognition by *Stb9* (Fig. 5c, d).

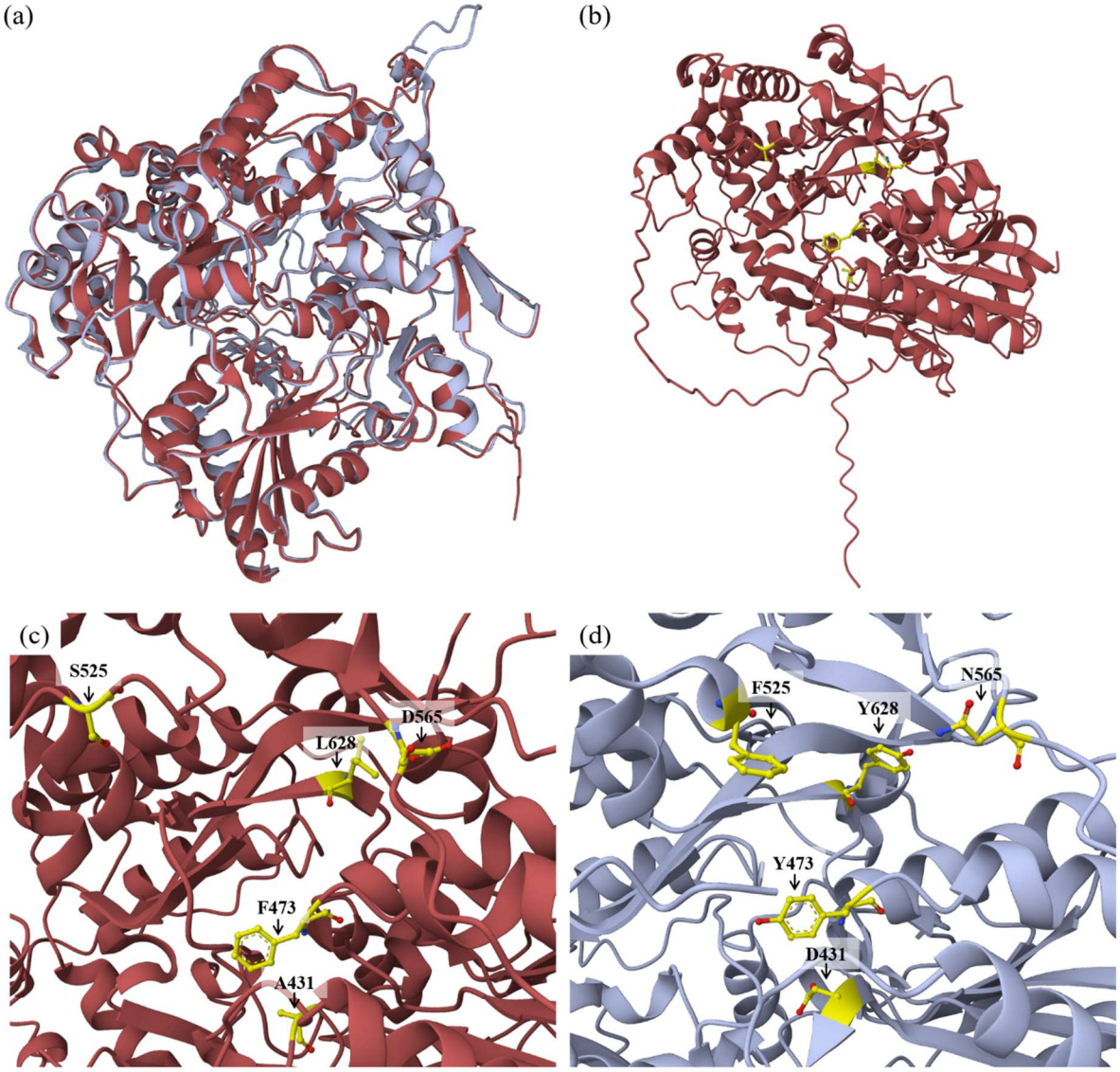


| | A431 | F473 | S525 | D565 | L628 |
|---|---|---|---|---|---|
| A431 | | | | | |
| F473 | 6.15 | | | | |
| S525 | 24.07 | 18.60 | | | |
| D565 | 20.41 | 15.76 | 18.77 | | |
| L628 | 17.61 | 12.53 | 19.00 | 12.73 | |

| | D431 | Y473 | F525 | N565 | Y628 |
|---|---|---|---|---|---|
| D431 | | | | | |
| Y473 | 6.29 | | | | |
| F525 | 19.75 | 13.97 | | | |
| N565 | 20.05 | 14.96 | 13.82 | | |
| Y628 | 16.72 | 12.23 | 17.22 | 12.62 | |

**Figure 5.** Three-dimensional structure of the protein AvrStb9 predicted with the ColabFold v1.5.2: AlphaFold2. (a) An overlay of the 3D structures of the virulent avrStb9 protein (isolate IPO323 in red) and of the avirulent AvrStb9 protein (isolate IPO09593 in blue). (b) The 3D structure of the virulent avrStb9 protein with the localization of the five residues potentially involved in virulence (highlighted in yellow). The (c) virulent avrStb9 and (d) avirulent AvrStb9 proteins with Top panel: zoom-in on the five residues in the 3D structure, and Bottom panel: distances (in Å) between the five residues.

269 In order to investigate *AvrStb9* diversity at a larger scale, we extended our analysis to include four global
270 *Z. tritici* populations. We found 44 different *AvrStb9* alleles in these populations, which translate to 38
271 different protein variants, mostly population-specific (Fig. 3c). Next, we analyzed *AvrStb9* nucleotide
272 diversity including ~500 bp of up- and downstream sequences from the start and stop codons,
273 respectively. We observed both a drop-in nucleotide diversity and Tajima's D in the *Avr* coding sequence
274 compared to the flanking regions (Fig. 3a). A negative Tajima's D is indicative of an excess of low
275 frequency polymorphisms, indicating population size expansion and/or selective sweeps.

276 The codon-based model analysis of *AvrStb9* coding sequence was used to investigate the selection
277 pressure exerted on the avirulence gene. Likelihood ratio tests (LRT) for different models indicated that
278 positive selection was highly probable, as selection models (M2 and M8) showed a significantly better
279 data fit compared to the neutral models M1 and M7 (Table S6). Selection analysis revealed 23 residues
280 (3.16% of the protein sequence) under positive diversifying selection (BEB probability > 0.95) in the
281 M2 model. Interestingly, S525F and L628Y, had the strongest positive selection probability (BEB
282 probability of = 1) among the five mutations potentially responsible of the virulence according to the
283 previous analyses (Table 1). We postulate that these adaptive mutations are under strong selective
284 pressure most probably to counteract recognition by the *Stb9* resistance gene.

285

286 **Discussion**

287 Gene-for-gene interactions in plant pathosystems are described when a host resistance gene recognizes
288 a pathogen's avirulence product that triggers a host immune response. Although 23 isolate-specific *Stb*
289 resistance genes have been mapped in wheat, only two have been cloned so far and their corresponding
290 fungal avirulence genes remain largely unknown. Here, we report the identification and characterization
291 of a novel avirulence gene, *AvrStb9*, which triggers complete resistance in wheat cultivars carrying *Stb9*
292 resistance gene. Additionally, we performed a high-resolution mapping of *Stb9* locus and delivered
293 tightly-linked SNP markers for its use in breeding.

294 *AvrStb9* is highly expressed during the asymptomatic phase of *Z. tritici* infection and drastically
295 downregulated upon the switch to the necrotrophic phase. In a previous study, *AvrStb9* was among the
296 top 100 highly expressed genes during the transition from biotroph to necrotrophy stage [26], suggesting
297 a function in host colonization during the asymptomatic phase or the transition to the necrotrophic phase.
298 The late recognition of *AvrStb9* could be indicative that the resistance gene inhibits the transition from
299 biotrophy to necrotrophy (*i.e.* inhibition of cell death). A useful means to verify this hypothesis is
300 through heterologous expression assays, which would help to understand how the *Avr* gene elicits *Stb9*-
301 dependent resistance. Recognition of the *Avr* allele leads to full resistance in cultivars carrying *Stb9*
302 following the gene-for-gene model. A previous study mapped the *Stb9* resistance locus to the long arm
303 of chromosome 2B but the genomic interval remained very large [24]. We used *AvrStb9* strain to trigger

304 wheat resistance and perform a precise mapping of the resistance locus, which revealed that *Stb9* resides
305 in the telomeric region of wheat chromosome 2B in an interval of 79.99-81.10Mb ($r^2 > 0.50$). Only two
306 STB resistance genes have been cloned to date, *Stb6* and *Stb16q*, both encoding receptor-like kinase
307 proteins [27,28], and our findings will help in the cloning of *Stb9* resistance gene.

308 *AvrStb9* is an atypical fungal avirulence gene, since it encodes a relatively large secreted protein (727
309 aa). Up to now, most of cloned avirulence genes from filamentous fungal pathogens encode small (<
310 300 aa), cysteine-rich secreted proteins. Only three exceptions to this rule are the *Ace1* gene from
311 *Magnaporthe grisea* [29] encoding a large polyketide synthase (PKS) fused to a nonribosomal peptide
312 synthetase (NRPS) likely involved in secondary metabolism, and two *AvrMla* genes from *Blumeria*
313 *graminis hordei* which encode large proteins [30]. Moreover, it appears that AvrStb9 has a predicted
314 protein domain corresponding to C-terminal processing S41 proteases, and show sequence similarities
315 with proteins from diverse fungal species. In plant pathogenic bacteria, some type III secreted effectors
316 injected in host plant cells are similar to catalytic enzymes involved in a variety of reactions such as E3
317 ligation or proteolysis [31]. For instance, *Pseudomonas syringae* secretes the cysteine protease *HopN1*
318 to suppress the host innate response and promote virulence [32].

319 The importance of proteases in fungal pathogenicity has previously been reported [33,34]. *Fusarium*
320 *oxysporum* f. sp. *lycopersicum* secretes a serine protease and a metalloprotease that cleave host
321 chitinases to prevent the degradation of fungal cell walls and facilitate host colonization [35]. The maize
322 anthracnose fungus *Colletotrichum graminicola* secretes a highly conserved metalloprotease effector
323 that enhances virulence [36]. Similarly, the rice blast fungus *Magnaporthe oryaze* secretes during
324 infection *Avr-Pita*, an effector protein with a predicted zinc metalloproteases domain that belongs to a
325 family of proteases that include other avirulence genes recognized by the resistance gene *Pi-ta* [37,38].
326 Our protein analyses (OrthoMCL, InterProScan, HHpred) indicated that AvrStb9 has sequence and
327 structural features typical of a protease. Protein structure-based homology searches identified the
328 secreted protease CPAF from the human pathogenic bacterium *C. trachomatis* as closest homolog.
329 CPAF degrades host transcription factors and therefore directly helps *Chlamydia* evading the host
330 defenses. One may speculate that AvrStb9 plays a similar role in proteolytic degradation of host protein
331 substrates. However, the enzymatic activity of AvrStb9 is yet to be investigated, as our analysis relied
332 primarily on sequence and structure comparisons. Further, the fact that we were hardly able to produce
333 *AvrStb9*-disrupted mutants indicates that the gene may play an important role in *Z. tritici* survival, and
334 that the proteolytic activity likely extends to include substrates essential for fungal growth.

335 The broad conservation of AvrStb9 in *Z. tritici* world population, its sister species and some other fungal
336 species suggested that this protein is a core effector shared among these lineages. Irieda *et al.* [39]
337 reported the conservation of *NIS1* effector that was initially detected from two *Colletotrichum* spp. in a
338 wide range of Ascomycota and Basidiomycota lineages. *NIS1* targets plant immune kinases to suppress

339 PAMP-triggered immunity [39]. We hypothesize that S41 proteases may have been anciently acquired
340 by fungi, and that the expansion of particular serine protease families is associated with the evolution of
341 fungal lifestyle. Indeed, S41 serine proteases are suspected to have a role in programmed cell death and
342 pathogenic life style adaptation in fungi [40]. We also identified multiple paralogs from multiple fungal
343 species, likely resulting from gene duplication events, highlighting either the redundancy of these genes
344 or their evolution to interact with different substrates. The functional redundancy of virulence genes has
345 been a technical challenge to study their biological functions, as disruption mutants often lead to the
346 conclusion that these genes are not essential for pathogenicity [41,42]. These redundancies may also
347 increase the organism's genetic robustness against null mutations or act in compensation of a gene loss
348 [43]. In *Z. tritici* for instance, the different *AvrStb9* paralogs had a secretion signal and show an
349 expression pattern consistent with a role as effectors. Taken altogether, we hypothesize that *AvrStb9* and
350 related S41 proteases constitute a set of core effectors gained early in the evolution of fungal-plant
351 interactions.

352 Recognition of effectors by host resistance exerts an evolutionary pressure that favors sequence
353 diversification, effector deletion or acquisition to counteract the immune response. We analyzed
354 AvrStb9 sequence diversity and found a broad conservation of its protein residues, unlike the other
355 known *Z. tritici* avirulence genes, *AvrStb6* and *Avr3D1* [44,18]. Nevertheless, we identified few
356 substitutions undergoing strong positive diversifying selection. Additional data from chimeric AvrStb9
357 transformants, from *Z. tritici* populations and from sequence conservation among the CPAF family
358 indicate S525 and L628 as probably the most important residues involved in virulence. Moreover, the
359 greater distance and the loss of polarity of residue S525 in the virulent form of avrStb9 may indicate the
360 importance of this residue in escaping recognition by *Stb9*, although we cannot exclude that
361 combinations of mutations may be necessary. Based on the structural model for CPAF function, one
362 may speculate that a functional protease is required to escape host recognition.

363 This is corroborated by the fact that, we did not observe in any of the global strains a loss of *AvrStb9* or
364 other deleterious mutations. Furthermore, *AvrStb9* deletion proved to be nearly impossible (only one
365 poorly growing transformant had the gene deletion out of the 271 tested). We therefore suggest that
366 *AvrStb9* plays an essential role in the biology of *Z. tritici*. Additional functional studies, including
367 mutating the S41 protease active sites in virulent and avirulent alleles will shed light on the role of the
368 protease activity of AvrStb9 in its diverse biological activities (fungal growth, wheat infection,
369 recognition by *Stb9*). But also, the function of the wheat resistance factor Stb9 is intriguing: Does it
370 work as classical receptor protein, recognizing the avirulent AvrStb9 protein or an AvrStb9-produced
371 peptide? Does it inhibit AvrStb9 protease activity? May the Stb9 resistance protein be the target of
372 AvrStb9 protease, or, on the contrary, does AvrStb9 targets a different protein that is "guarded" by Stb9
373 resistance?

374 In conclusion, we identified a new major avirulence factor of *Z. tritici* that triggers an immune response
375 in hosts carrying the corresponding resistance gene. Unlike what has been described for most avirulence
376 genes, *AvrStb9* encodes a large protein with a predicted protease domain and likely belongs to a family
377 of conserved fungal S41 proteases. This is an important step in deciphering molecular mechanisms
378 underlying wheat – *Z. tritici* interactions, and shed light on the role of 'atypical' effectors in fungal
379 avirulence. It opens new research avenues to broaden our knowledge on host-pathogen interactions, in
380 particular the characterization of enzyme activity of effectors, which will greatly help our understanding
381 of the biology of protease effectors, commonly found in fungal pathogens.

382

383 ## Materials and Methods

384 ### Fungal material

385 A total of 103 *Z. tritici* strains were used for GWAS analysis. The strains derive from a French *Z. tritici*
386 collection collected in 2009 on cultivars 'Apache' (n = 44), 'Premio' (n = 42), 'Soissons' (n = 9),
387 'Caphorn' (n = 3), 'Alixan' (n = 1), 'Bermude' (n = 1), 'Dinosaur' (n = 1) and 'Garcia' (n = 1); one
388 isolate was collected in the UK on cultivar 'Humbert'. The two isolates used for genetic mapping of the
389 resistance and fungal transformation are IPO323 and IPO09593. IPO323 is a Dutch isolate collected on
390 cultivar 'Arminda' in 1981 and used as the reference strain for *Z. tritici* [45]. IPO09593 is part of the
391 103 strains and has been isolated from 'Apache' in 2009. IPO323 is virulent on cultivars carrying *Stb9*
392 resistance gene while IPO09593 is avirulent on *Stb9*-cultivars. The three additional isolates used to
393 construct deletion and allele swap transformants, namely IPO09359 ('Apache', 2009), IPO09139
394 ('Apache', 2009) and SYN32 (unknown cultivar, 2006), are avirulent on *Stb9*-cultivars.

395 ### Plant material

396 We performed quantitative trait loci (QTL) mapping in a recombinant doubled haploid (DH) population
397 comprised of 65 lines, developed from the $F_1$ progeny of the cultivars 'Beaver' and 'Soissons' [46]. A
398 panel of 220 modern French bread wheat (BW) varieties was used for GWAS analysis; details on the
399 BW panel used here can be found in [47]. We also characterized *Z. tritici* wild-type and mutant strains
400 on near isogenic lines (NILs) carrying or not the *Stb9* resistance gene in the genetic background of
401 cultivar 'Courtot', developed at INRAE GDEC (Clermont-Ferrand, France). The 'Courtot' NILs were
402 developed following three backcrosses starting with $F_1$ 'Courtot' x 'Chinese spring' (carrying a
403 susceptible allele of *Stb9* gene). To keep the *Stb9* susceptible allele in the progenies, each plant was
404 genotyped with single sequence repeat markers wmc317 and barc129 and phenotyped with the *Stb9*
405 avirulent isolate IPO89011. A $BC_3F_1$ plant heterozygous at the *Stb9* locus was self-fertilized. $BC_3F_2$
406 plants homozygous either for the susceptible *Stb9* allele ('Courtot' – Stb9) or for the resistant allele
407 ('Courtot' + Stb9) were selfed and constitute the 'Courtot' NILs.

408 **Pathogenicity assays**

409 Pathogenicity assays were performed following the procedure described by [21]. Briefly, 16 days old
410 plants were marked to delimit a 75 mm segment on the first true leaf. The segment was inoculated with
411 a paintbrush dipped into a $10^6$ spores.mL$^{-1}$ inoculum solution with one drop of Tween20 added per 15
412 mL. After inoculation, the plants were watered and covered with transparent polyethylene bags for 72
413 hours to initiate the infection. The plants were kept in a climate chamber with a 16 h photoperiod (300
414 µmol.m$^{-2}$.s$^{-1}$), 80-90% relative humidity and 18°C night/22°C day. Phenotyping of the fungal population
415 was performed by visually assessing strain virulence on the cultivar 'Soissons' at 21 days post
416 inoculation (dpi). Visual assessments were made of percent of leaf area covered by necrosis (PLACN)
417 and by pycnidia (PLACP) within the inoculated segment of each leaf (disease scale available at Fig. S8).
418 Each of the 103 strains was tested in three replicates with three leaves per replicate. Phenotyping of
419 *AvrStb9* mutant strains was performed following the same procedure.

420 For the host mapping populations, the Beaver/Soissons DH lines were inoculated with the strain
421 IPO09593, and the 220 wheat varieties were inoculated with the strains IPO09593 and IPO323. Here,
422 each interaction was tested in two replicates with three leaves per replicate and visual assessments of
423 PLACN and PLACP were recorded at 14, 20 and 26 dpi. We calculated the area under disease progress
424 curve for necrosis (AUDPCn) and sporulation (AUDPCs) with the formula:

425 $$\mathrm{AUDPC} = \frac{\sum[(t_{i+1} - t_i) \times (y_i + y_{i+1})]}{2}$$

426 With, $t_{i+1}-t_i$: number of days between two observations; $y_i$: PLACN or PLACP at day i; $y_{i+1}$: PLACN or
427 PLACP at day i+1. AUDPC were calculated relative to their maximum theoretical value, RAUDPCn
428 and RAUDPCs respectively. For all assays, disease severity data were averaged between replicates and
429 used as the input phenotype in GWAS and QTL analyses.

430 **Fungal whole-genome sequencing and variant calling**

431 Fungal spores were obtained after 7 days growth in liquid cultures of yeast extract-peptone-dextrose
432 Broth (Difco YPD Broth), and then freezed-dried during 24 h. High molecular weight DNA was
433 extracted using a phenol-chloroform based procedure. Illumina paired-end libraries were prepared for
434 each sample and DNA fragments sequenced with 2x100 bp reads on a HiSeq-2000 sequencing system
435 at Genewiz, Inc. (formerly Beckman Coulter Genomics). Depth of sequence coverage was variable
436 depending on the isolate, ranging from 16 to 303 genome equivalents with an average of 61 genome
437 equivalents. For each strain, reads were trimmed using trimmomatic v0.32 [48] and then mapped on the
438 reference genome IPO323 [45] using the mem algorithm from BWA v0.7.7 [49] with default options.
439 Samtools v0.1.19 and Picard tools v1.106 [50] were used to filter reads (optic duplicates, secondary
440 alignments and reads with a mapping quality < 30) and keep only pairs in which both reads met quality
441 checks. SNP calling was done with Freebayes v0.9 with the option --report-monomorphic [51]. All
442 positions detected as low-complexity regions or transposable elements (TE) were excluded using

443 RepeatMasker 4.0 with default options and REPET [52], respectively. Quality filters were applied on
444 the gVCF using in-house scripts. Depth of coverage (DP) calculated at each position follows a normal
445 distribution around the depth main peak; a DP filter was set at twice the standard deviation from the
446 mean. All the gVCF were stored into a matrix reduced to keep only the positions where at least one
447 strain has a detected SNP in a non-filtered position. The SNP matrix was parsed in .tped format,
448 converted to .ped/.map and filtered for < 0.5 missing data and > 0.1 minor allele frequency (MAF) using
449 PLINK v.1.9 [53].

450 **GWAS analyses**

451 For Genome-Wide Association Analysis (GWAS), we used the linear mixed model implemented in the
452 R package 'GAPIT' [54]. To account for population structure and reduce spurious associations, a kinship
453 matrix using the VanRaden method and the first three principal components computed from SNP data
454 were included a covariate in the model. We used a Bonferroni threshold of $p < 2.67e\text{-}7$ ($\alpha$=0.05) to
455 declare significant SNPs associated with phenotypic variations. Linkage Disequilibrium (LD) measures
456 ($r^2$) for the significant SNPs were obtained with PLINK v.1.9 using the --r2 command and LD blocks
457 were visualized using the R package 'LDheatmap'. SNPs with an $r^2 \geq 0.5$ were considered in strong LD.

458 **Genetic mapping of *Stb9***

459 A genetic linkage map was available for the Beaver/Soissons DH population and contains 312
460 polymorphic loci: 121 SSR, 49 AFLP, 135 DArT markers and 7 major genes [46]. The map covers 1,526
461 cM with an average density of one marker per 12.6 cM. QTL mapping was conducted using RAUDPCs
462 and RAUDPCn phenotypes obtained from the isolate IPO09593 (*AvrStb9*) with R/qtl software v.1.48-1
463 [55]. Linkage analysis was performed for each trait with an initial Simple Interval Mapping (SIM),
464 followed by a Composite Interval Mapping (CIM). For SIM, 1000 genome-wide permutations were used
465 to calculate the significant logarithm of odds (LOD) threshold. Only QTLs that showed *p*-values less
466 than 0.05 were considered significant. Association mapping in the BW panel was done following the
467 exact same procedure as in the fungal population (see GWAS analyses). The 220 BW varieties have
468 been previously genotyped on an Affymetrix Axiom 410K single nucleotide polymorphism (SNP) array
469 [56]. Procedure of allele calling, filtering and quality check of genotype data are described in Balfourier
470 *et al.* [57]. For GWAS analysis, we excluded markers with less than 5% minor allele frequency and
471 more than 10% missing data and kept a set of 186,961 SNPs that passed quality control criteria and
472 could be anchored on the IWGSC annotation v2.1 [58]. We used filtered SNP data and phenotypes
473 (RAUDPCs and RAUDPCn) from the isolates IPO323 (*avrStb9*) and IPO09593 (*AvrStb9*) to perform
474 marker-trait associations.

475 **Gene annotation and expression analysis**

476 Predicted genes in the candidate region were retrieved from the *Z. tritici* reference genome annotation
477 [59]. We used RNA-seq data [23] mapping onto the reference genome IPO323 to manually curate

478 *Zt_1_693* (*AvrStb9)* gene model. Canonical and non-canonical splicing sites were confirmed by *de-novo*
479 transcriptome assembly obtained with DRAP [60]. The final gene model differed from those from
480 previous annotations due to errors in predicting correctly introns and includes two missing exons.
481 Candidate genes were screened for the presence of a secretion signal using SignalP 3.0 server [61].
482 Blastp was used to search for *AvrStb9* orthologous and paralogous proteins against the reference strain
483 IPO323 and closely-related *Zymoseptoria* species. Protein domains were searched using Interproscan
484 and structure homology prediction was performed in the HHpred server;
485 <https://toolkit.tuebingen.mpg.de/tools/hhpred>. For gene expression analysis, RNA-seq data samples
486 from *in vitro* and *in planta* (1, 4, 9, 14 and 21 dpi) conditions were obtained from Rudd *et al.* [23], and
487 gene expression quantified as fragments per kilobase of exon per million fragments mapped (FPKM)
488 using Cuffdiff v.2.2.1 [62]. *AvrStb9* DNA sequences are deposited in NCBI Genbank (accession
489 numbers OP376566 and OP376567).

490 **Prediction and comparison of protein structures**

491 The virulent avrStb9 and avirulent AvrStb9 (from isolates IPO323 and IPO09593, respectively) mature
492 protein structures (i.e. without the signal peptide) were predicted with the ColabFold v1.5.2: AlphaFold2
493 using MMseqs2 with default parameters [63,64]. Structural similarity searches against the full Protein
494 Data Bank (PDB) [65] were performed using the DALI webserver available at
495 <http://ekhidna2.biocenter.helsinki.fi/dali/> [66]. Sequences and structures of the CPAF homodimer
496 were extracted from the PDB with accession numbers 3DOR-A and 3DOR-B [25]. To further investigate
497 similarities between protein tertiary structures, the RCSB PDB website
498 <https://www.rcsb.org/alignment> [67] was used to align AvrStb9 against avrStb9 and AvrStb9 against
499 CPAF (chains A and B) using the TM-align algorithm [68]. All images of 3D structures and structure
500 superposition were captured and analyzed using Mol* Viewer <https://www.rcsb.org/3d-view> [69].
501 Finally, the five residues possibly associated with virulence were highlighted on the protein structures
502 and distances between residues on both avrStb9 and AvrStb9 proteins were calculated using the
503 measurement option of Mol* Viewer.

504 **Construction of disruption plasmids**

505 For *AvrStb9* disruption, the hygromycin resistance marker (*hph*) was cloned between the 1,000 bp up-
506 and downstream flanking regions of the ORF, respectively. The following DNA fragments were
507 generated and cloned into pCAMBIA0380 plasmids (GenBank: AF234290.1). The up- and downstream
508 flanks were obtained by PCR on gDNA of IPO323 with primer pairs 1&2 and 5&6 (Table S7)
509 respectively using Q5 Hot Start High fidelity DNA polymerase (NEB, Evry, France). The *hph* was
510 amplified from pCAMBIA0380 with the primers 3 and 4 (Table S7). pCAMBIA0380 was digested by
511 *Eco*RI and *Xho*I and used for the cloning of three PCR fragments with Gibson Assembly cloning kit
512 (NEB, Evry, France) according to the supplier's indications. The ligation product was introduced into

513 NEB 5α competent *Escherichia coli* cells (NEB, Evry, France), transformants selected on kanamycin
514 (50 µg.mL$^{-1}$) containing LB-broth. Colonies were screened by PCR with the primer-pairs used for
515 cloning. Four positive colonies were chosen for plasmid extraction (Macherey & Nagel, Düren,
516 Germany) and restriction analysis. The construct was then introduced by electroporation into the
517 *Agrobacterium tumefaciens* Agl1 strain. Transformants were selected and isolated on YEB (5 g. L$^{-1}$ beef
518 extract, 1 g. L$^{-1}$ yeast extract, 5 g. L$^{-1}$ peptone, 5 g. L$^{-1}$ sucrose, 0.5 g. L$^{-1}$ MgCl2, 1.5% agar) with
519 kanamycin (50 µg. mL$^{-1}$).

520 **Gene replacement constructs**

521 To swap *AvrStb9* alleles between virulent (IPO323) and avirulent (IPO09593) strains, the following
522 replacement cassettes were constructed. The respective *AvrStb9* alleles were amplified with primers 11
523 and 12 (Table S7) from IPO323 or IPO09593 gDNA. These fragments cover the ORF with 1 kb
524 upstream of the START codon and 360 bp downstream of the STOP codon. The *hph* (amplified with
525 primers 9 and 10 from pCAMBIA0380 plasmid DNA) and the 1 kb upstream flank of *AvrStb9* gene
526 (amplified with primers 7 and 8) were ligated to *AvrStb9* alleles into the *EcoRI-XhoI* digested
527 pCAMBIA0380, with Gibson Assembly cloning kit (NEB, Evry, France). Plasmids were introduced
528 into NEB 5α competent *E. coli* cells (NEB, Evry, France) and transformants selected on kanamycine
529 (50 µg.mL$^{-1}$) containing LB-broth. Colonies were screened by PCR with the primer-pairs used for
530 cloning. Four positive colonies were chosen for plasmid extraction (Macherey & Nagel, Düren,
531 Germany) and sequence analysis. These constructs named respectively pR323 and pR9593 were then
532 introduced by electroporation into the *Agrobacterium tumefaciens* Agl1 strain. Transformants were
533 selected and isolated on YEB with kanamycin (50 µg.mL$^{-1}$).

534 **Generation of *Z. tritici* transformants**

535 The transformation procedure was adapted from Zwiers & de Waard [70] and was performed as
536 previously described [71]. For *AvrStb9* deletion, the following *Z. tritici* strains were transformed with
537 the disruption plasmid: IPO323, IPO09593, IPO09359, IPO09139 and SYN32. Transformants were
538 selected and isolated twice on hygromycin (100 µg. mL$^{-1}$) containing medium. The replacement of the
539 *AvrStb9* ORF by the *hph* gene was checked by PCR on gDNA with the primer pair 13 and 14. The gene
540 deletion is expected to give a 1.6 kb fragment instead of the native 2.4 kb amplicon. The total number
541 of isolated and analyzed transformants were: IPO323 (n=144), IPO09593 (n=23), IPO09359 (n=26),
542 IPO09139 (n=46), SYN32 (n=38). One single transformant produced the expected PCR profile, namely
543 SYN32_ΔT12.

544 For *AvrStb9* allele swaps, IPO323 was transformed with plasmids pR323 and pR9593. Transformants
545 selected and isolated twice on hygromycin containing medium (100 µg. mL$^{-1}$). The replacement of
546 *AvrStb9* alleles in the transformants was checked by PCR using primers 15 and 16, leading to a single
547 1.6 kb amplicon in replacement mutants and to an additional 238 bp amplicon in ectopic transformants.

548 Transformants with the expected single band size were PCR checked with primers 17 and 18 as these
549 primers allow to distinguish the deletion of the amino acid residues 66-71 in the IPO09593 background
550 from the IPO323 one, and subsequently submitted to sequence analysis with primers indicated in Table
551 S7.

552 **Phylogenetic analysis.**

553 We used OrthoMCL algorithm to search for *AvrStb9* orthologous and paralogous protein sequences
554 using a cutoff E-value less than 1e-20 and filtering for low complexity regions [72];
555 <https://orthomcl.org/orthomcl/app/>. Of the 148 putative *AvrStb9* orthologs/paralogs identified
556 through OrthoMCL, we selected 122 by removing redundant information using the following criteria:
557 (*i*) when multiple identical sequences were present, one was arbitrarily chosen and retained; and (*ii*)
558 when multiple sequences from different strains of the same species were present, an arbitrarily chosen
559 strain (the reference strain, if known) was retained. A multiple sequence alignment was then generated
560 with Clustal Omega v1.2.4 [73] and alignment cleaning was performed using trimAL with the --
561 gappyout option [74]. We constructed a maximum likelihood tree of selected *AvrStb9* orthologs/paralogs
562 using RaxML with the GAMMA JTT model and 100 bootstrap replicates [75]. Phylogenetic trees were
563 visualized using iTOL [76]; <https://itol.embl.de/>.

564 **Population genetics and selection analyses**

565 In addition to the fungal population used for genetic analyses, we extended our sequence diversity and
566 selection analyses to include a global *Z. tritici* population originating from four distinct geographic
567 locations, including the middle East (n=30, Israel), Australia (n=27, Wagga Wagga), Europe (n=33,
568 Switzerland) and North America (n=56, Oregon, USA). Procedures of *de novo* genome assemblies and
569 sequence extraction were previously described [77]. We used DnaSP v6 [78] to calculate summary
570 statistics of the population genetic parameters associated with *AvrStb9*. Sliding window analyses of
571 nucleotide diversity ($\pi$) and Tajima's D were conducted in a window length of 200 bp and a step size of
572 20 bp. To test the selective pressure acting on *AvrStb9*, we estimated the rates of non-synonymous (dN)
573 and synonymous (dS) substitutions using CodeML from the PAML package [79]. A dN/dS ($\omega$) ratio of
574 1 indicated neutrality, whereas $\omega < 1$ or $> 1$ suggested purifying or diversifying selection, respectively.
575 However, the presence of intragenic recombination could bias the $\omega$ rate testing. To account for these
576 issues, we performed the analysis with a non-recombining phylogenetic tree generated from the RDP4
577 software using RaxML with 100 bootstraps [80].

578

579 **Data Availability**

580 Genome sequencing data for the 103 French *Z. tritici* isolates is available at NCBI BioProject
581 PRJNA777581 (accessions SRR16762555 to SRR16762657). *AvrStb9* gene sequences are available at
582 NCBI Genbank (accession numbers OP376566 and OP376567).

**Acknowledgements**

We thank David Gouache, Henriette Goyeau, Gert H.J. Kema, Marc-Henri Lebrun, Frédéric Suffert and Anne-Sophie Walker for their contribution in establishing the fungal population; Johann Confais for his help in the virulence assays; Robert King and Jason Rudd for providing IPO323 RNA-seq data; Florence Cambon, the VégéPôle and GENTYANE platforms for the development of the Courtot NILs; Marc-Henri Lebrun for critical reading of the manuscript and valuable feedback; and Sophie Bouchet and Fanny Hartmann for assistance with the initial GWAS analyses.

**Financial Disclosure**

T.C.M. received support from the French Fund to support Plant Breeding (FSOV 2008 H). J.A. and T.C.M. received support from the French National Research Agency (program BIOADAPT, grant no. ANR-12-ADAP-0009-04), including the salary of J.C. S. F. and T.C.M received support from BASF France SAS (V.I.S.A. project), including the salary of R.A. INRAE BIOGER benefits from the support of Saclay Plant Sciences-SPS (ANR-17-EUR-0007). The funders had no role in study design, data collection and analysis, decision to publish, or preparation of the manuscript.

**Author Contributions**

**Conceptualization**: Sabine Fillinger, Thierry C. Marcel.

**Data curation**: Nicolas Lapalu.

**Formal analysis**: Reda Amezrou, Jérôme Compain, Nicolas Lapalu, Clémentine Louet, Daniel Croll, Sabine Fillinger, Thierry C. Marcel.

**Funding acquisition**: Joëlle Amselem, Sabine Fillinger, Thierry C. Marcel.

**Investigation**: Reda Amezrou, Colette Audéon, Sandrine Gélisse, Aurélie Ducasse, Clémentine Louet, Sabine Fillinger, Thierry C. Marcel.

**Project administration**: Joëlle Amselem, Thierry C. Marcel.

**Resources**: Cyrille Saintenac, Simon Orford, Daniel Croll.

**Supervision**: Joëlle Amselem, Sabine Fillinger, Thierry C. Marcel.

**Validation**: Reda Amezrou, Sabine Fillinger, Thierry C. Marcel.

**Visualization**: Reda Amezrou, Clémentine Louet, Thierry C. Marcel.

**Writing – original draft:** Reda Amezrou.

**Writing – review & editing:** Reda Amezrou, Cyrille Saintenac, Nicolas Lapalu, Clémentine Louet, Daniel Croll, Sabine Fillinger, Thierry C Marcel.

616 **References**


617 [1] Savary S, Willocquet L, Pethybridge SJ, Esker P, McRoberts N, Nelson A. The global burden of
618 pathogens and pests on major food crops. Nat Ecol Evol. 2019; 3: 430–439.

619 [2] Lo Presti L, Lanver D, Schweizer G, Tanaka S, Liang L, Tollot M, *et al.* Fungal effectors and plant
620 susceptibility. Annu Rev Plant Biol. 2015; 66: 513–545.

621 [3] Rocafort M, Fudal I, Mesarich CH. Apoplastic effector proteins of plant-associated fungi and
622 oomycetes. Curr Opin Plant Biol. 2020; 56: 9-19.

623 [4] Jones JDG, Dangl JL. The plant immune system. Nature. 2006; 444: 323–329.

624 [5] Flor HH. The complementary genic systems in flax and flax rust**Joint contribution from the Field
625 Crops Research Branch, Agricultural Research Service, United States Department of Agriculture and
626 the North Dakota Agricultural Experiment Station. In: Demerec MBT-A in G, ed. Academic Press; 1956.
627 pp. 29–54.

628 [6] Sánchez-Vallet A, Fouché S, Fudal I, Hartmann FE, Soyer JL, Tellier A, Croll D. The genome biology
629 of effector gene evolution in filamentous plant pathogens. Annu Rev Phytopathol. 2018; 56: 21-40.

630 [7] Stergiopoulos I, de Wit PJGM. Fungal effector proteins. Annu Rev Phytopathol. 2009; 47: 233–263.

631 [8] Franceschetti M, Maqbool A, Jiménez-Dalmaroni MJ, Pennington HG, Kamoun S, Banfield MJ.
632 Effectors of filamentous plant pathogens: commonalities amid diversity. Microbiol Mol Biol Rev. 2017;
633 81: e00066–16.

634 [9] de Guillen K, Ortiz-Vallejo D, Gracy J, Fournier E, Kroj T, Padilla A. Structure analysis uncovers a
635 highly diverse but structurally conserved effector family in phytopathogenic fungi. PLOS Pathog 2015;
636 11(10): e1005228.

637 [10] Lazar N, Mesarich CH, Petit-Houdenot Y, Talbi N, Li de la Sierra-Gallay I, Zélie E, *et al*. A new family
638 of structurally conserved fungal effectors displays epistatic interactions with plant resistance proteins.
639 PLOS Pathog 2022; 18(7): e1010664.

640 [11] Seong K, Krasileva KV. Prediction of effector protein structures from fungal phytopathogens
641 enables evolutionary analyses. Nat Microbiol 2023; 8(1): 174-187.

642 [12] Petit-Houdenot Y, Lebrun MH, Scalliet G. Understanding plant-pathogen interactions in Septoria
643 tritici blotch infection of cereals. In: Achieving durable disease resistance in cereals. London, UK:
644 Burleigh Dodds Science Publishing; 2021. pp. 263-302.

645 [13] Battache M, Lebrun MH, Sakai K, Soudière O, Cambon F, Langin T, Saintenac C. Blocked at the
646 stomatal gate, a key step of wheat Stb16q-mediated resistance to *Zymoseptoria tritici*. Front Plant Sci.
647 2022; 13: 921074.

648 [14] Sánchez-Vallet A, McDonald MC, Solomon PS, McDonald BA. Is *Zymoseptoria tritici* a
649 hemibiotroph? Fungal Genet Biol. 2015; 79: 29–32.

650 [15] Fones H, Gurr S. The impact of Septoria tritici blotch disease on wheat: An EU perspective. Fungal
651 Genet Biol. 2015; 79: 3–7.

652 [16] Zhong Z, Marcel TC, Hartmann FE, Ma X, Plissonneau C, Zala M, *et al*. A small secreted protein in
653 *Zymoseptoria tritici* is responsible for avirulence on wheat cultivars carrying the *Stb6* resistance gene.
654 New Phytol. 2017; 214: 619–631.

655 [17] Kema GHJ, Mirzadi Gohari A, Aouini L, Gibriel HAY, Ware SB, van den Bosch F, *et al*. Stress and
656 sexual reproduction affect the dynamics of the wheat pathogen effector *AvrStb6* and strobilurin
657 resistance. Nature Genet. 2018; 50: 375–380.

658 [18] Meile L, Croll D, Brunner PC, Plissonneau C, Hartmann FE, McDonald BA, Sánchez-Vallet A. A fungal
659 avirulence factor encoded in a highly plastic genomic region triggers partial resistance to Septoria tritici
660 blotch. New Phytol. 2018; 219: 1048–1061.

661 [19] Brown JKM, Chartrain L, Lasserre-Zuber P, Saintenac C. Genetics of resistance to *Zymoseptoria*
662 *tritici* and applications to wheat breeding. Fungal Genet Biol. 2015; 79: 33–41.

663 [20] Yang N, McDonald MC, Solomon PS, Milgate AW. Genetic mapping of *Stb19*, a new resistance gene
664 to *Zymoseptoria tritici* in wheat. Theor Appl Genet. 2018; 131: 2765–2773.

665 [21] Langlands-Perry C, Cuenin M, Bergez C, Ben Krima S, Gélisse S, Sourdille P, *et al*. Resistance of the
666 wheat cultivar 'Renan' to Septoria leaf Blotch explained by a combination of strain specific and strain
667 non-specific QTL mapped on an ultra-dense genetic map. Genes. 2022; 13: 100.

668 [22] Suffert F, Sache I, Lannou C. Assessment of quantitative traits of aggressiveness in *Mycosphaerella*
669 *graminicola* on adult wheat plants. Plant Pathol. 2013; 62: 1330–1341.

670 [23] Rudd JJ, Kanyuka K, Hassani-Pak K, Derbyshire M, Andongabo A, Devonshire J, *et al*. Transcriptome
671 and metabolite profiling of the infection cycle of *Zymoseptoria tritici* on wheat reveals a biphasic
672 interaction with plant immunity involving differential pathogen chromosomal contributions and a
673 variation on the hemibiotrophic lifestyle definition. Plant Physiol. 2015; 167: 1158–1185.

674 [24] Chartrain L, Sourdille P, Bernard M, Brown JKM. Identification and location of *Stb9*, a gene for
675 resistance to Septoria tritici blotch in wheat cultivars Courtot and Tonic. Plant Pathol. 2009; 58: 547–
676 555.

677 [25] Huang Z, Feng Y, Chen D, Wu X, Huang S, Wang X, *et al*. Structural basis for activation and inhibition
678 of the secreted chlamydia protease CPAF. Cell Host Microbe. 2008; 4: 529-42.

679 [26] Palma-Guerrero J, Ma X, Torriani SFF, Zala M, Francisco CS, Hartmann FE, *et al*. Comparative
680 transcriptome analyses in *Zymoseptoria tritici* reveal significant differences in gene expression among
681 strains during plant infection. Mol Plant-Microbe Interact. 2017; 30: 231–244.

682 [27] Saintenac C, Lee W-S, Cambon F, Rudd JJ, King RC, Marande W, *et al*. Wheat receptor-kinase-like
683 protein *Stb6* controls gene-for-gene resistance to fungal pathogen *Zymoseptoria tritici*. Nature Genet.
684 2018; 50: 368–374.

685 [28] Saintenac C, Cambon F, Aouini L, Verstappen E, Ghaffary SMT, Poucet T, *et al*. A wheat cysteine-
686 rich receptor-like kinase confers broad-spectrum resistance against Septoria tritici blotch. Nat
687 Commun. 2021; 12: 433.

688 [29] Collemare J, Pianfetti M, Houlle A-E, Morin D, Camborde L, Gagey M-J, *et al. Magnaporthe grisea*
689 avirulence gene *ACE1* belongs to an infection-specific gene cluster involved in secondary metabolism.
690 New Phytol. 2008; 179: 196–208.

691 [30] Bourras S, McNally KE, Müller MC, Wicker T, Keller B. Avirulence genes in cereal powdery mildews:
692 the gene-for-gene hypothesis 2.0. Front Plant Sci. 2016; 7: 241.

693 [31] Hann DR, Gimenez-Ibanez S, Rathjen JP. Bacterial virulence effectors and their activities. Curr Opin
694 Plant Biol. 2010; 13: 388–393.

695 [32] López-Solanilla E, Bronstein PA, Schneider AR, Collmer A. HopPtoN is a *Pseudomonas syringae* Hrp
696 (type III secretion system) cysteine protease effector that suppresses pathogen-induced necrosis
697 associated with both compatible and incompatible plant interactions. Mol Microbiol. 2004; 54: 353–
698 365.

699 [33] Jashni MK, Mehrabi R, Collemare J, Mesarich CH, de Wit PJGM. The battle in the apoplast: Further
700 insights into the roles of proteases and their inhibitors in plant–pathogen interactions. Frontiers Plant
701 Sci. 2015; 6: 584.

702 [34] Chandrasekaran M, Thangavelu B, Chun SC, Sathiyabama M. Proteases from phytopathogenic
703 fungi and their importance in phytopathogenicity. J Gen Plant Pathol. 2016; 82: 233–239.

704 [35] Jashni MK, Dols IHM, Iida Y, Boeren S, Beenen HG, Mehrabi R, *et al*. Synergistic action of a
705 metalloprotease and a serine protease from *Fusarium oxysporum* f. sp. *lycopersici* cleaves chitin-
706 binding tomato chitinases, reduces their antifungal activity, and enhances fungal virulence. Mol Plant-
707 Microbe Interact. 2015; 28: 996–1008.

708 [36] Sanz-Martín JM, Pacheco-Arjona JR, Bello-Rico V, Vargas WA, Monod M, Díaz-Mínguez JM, *et al*.
709 A highly conserved metalloprotease effector enhances virulence in the maize anthracnose fungus
710 *Colletotrichum graminicola*. Mol Plant Pathol. 2016; 17: 1048–1062.

711 [37] Orbach MJ, Farrall L, Sweigard JA, Chumley FG, Valent B. A telomeric avirulence gene determines
712 efficacy for the rice blast resistance gene *Pi-ta*. Plant Cell. 2000; 12: 2019–2032.

713 [38] Khang CH, Park S-Y, Lee Y-H, Valent B, Kang S. Genome organization and evolution of the *AVR-Pita*
714 avirulence gene family in the *Magnaporthe grisea* species complex. Mol Plant-Microbe Interact. 2008;
715 21: 658–670.

716 [39] Irieda H, Inoue Y, Mori M, Yamada K, Oshikawa Y, Saitoh H, *et al*. Conserved fungal effector
717 suppresses PAMP-triggered immunity by targeting plant immune kinases. Proc Natl Acad Sci USA.
718 2019; 116: 496–505.

719 [40] Muszewska A, Stepniewska-Dziubinska MM, Steczkiewicz K, Pawlowska J, Dziedzic A, Ginalski K.
720 Fungal lifestyle reflected in serine protease repertoire. Sci Rep. 2017; 7: 9147.

721 [41] Plummer KM, Clark SJ, Ellis LM, Loganathan A, Al-Samarrai TH, Rikkerink EHA, *et al*. Analysis of a
722 secreted aspartic peptidase disruption mutant of *Glomerella cingulata*. Eur J Plant Pathol. 2004; 110:
723 265–274.

724 [42] ten Have A, Espino JJ, Dekkers E, van Sluyter SC, Brito N, Kay J, *et al*. The *Botrytis cinerea* aspartic
725 proteinase family. Fungal Genet Biol. 2010; 47: 53–65.

726 [43] Gu Z, Steinmetz LM, Gu X, Scharfe C, Davis RW, Li W-H. Role of duplicate genes in genetic
727 robustness against null mutations. Nature. 2003; 421: 63–66.

728 [44] Brunner PC, McDonald BA. Evolutionary analyses of the avirulence effector *AvrStb6* in global
729 populations of *Zymoseptoria tritici* identify candidate amino acids involved in recognition. Mol Plant
730 Pathol. 2018; 19: 1836–1846.

731 [45] Goodwin SB, Ben M'Barek S, Dhillon B, Wittenberg AHJ, Crane CF, Hane JK, *et al.* Finished genome
732 of the fungal wheat pathogen *Mycosphaerella graminicola* reveals dispensome structure,
733 chromosome plasticity, and stealth pathogenesis. PLoS Genet. 2011; 7: e1002070.

734 [46] Singh D, Simmonds J, Park RF, Bariana HS, Snape JW. Inheritance and QTL mapping of leaf rust
735 resistance in the European winter wheat cultivar 'Beaver.' Euphytica. 2009; 169: 253–261.

736 [47] Touzy G, Rincent R, Bogard M, Lafarge S, Dubreuil P, Mini A, *et al.* Using environmental clustering
737 to identify specific drought tolerance QTLs in bread wheat (*T. aestivum* L.). Theor Appl Genet. 2019;
738 132: 2859-2880.

739 [48] Bolger AM, Lohse M, Usadel B. Trimmomatic: a flexible trimmer for Illumina sequence data.
740 Bioinformatics. 2014; 30: 2114–2120.

741 [49] Li H, Durbin R. Fast and accurate short read alignment with Burrows–Wheeler transform.
742 Bioinformatics. 2009; 25: 1754–1760.

743 [50] Li H, Handsaker B, Wysoker A, Fennell T, Ruan J, Homer N, *et al*. The Sequence Alignment/Map
744 format and SAMtools. Bioinformatics. 2009; 25: 2078–2079.

745 [51] Garrison E, Marth G. Haplotype-based variant detection from short-read sequencing. arXiv:
746 1207.3907v2. [Preprint]. 2012 [cited 2022 November 17]. Available from:
747 https://doi.org/10.48550/arXiv.1207.3907

748 [52] Flutre T, Duprat E, Feuillet C, Quesneville H. Considering transposable element diversification in
749 *de novo* annotation approaches. PLoS One. 2011; 6: e16526.

750 [53] Chang CC, Chow CC, Tellier LCAM, Vattikuti S, Purcell SM, Lee JJ. Second-generation PLINK: rising
751 to the challenge of larger and richer datasets. GigaScience. 2015; 4: 7.

752 [54] Lipka AE, Tian F, Wang Q, Peiffer J, Li M, Bradbury PJ, *et al*. GAPIT: genome association and
753 prediction integrated tool. Bioinformatics. 2012; 28: 2397–2399.

754 [55] Broman KW, Wu H, Sen Ś, Churchill GA. R/qtl: QTL mapping in experimental crosses.
755 Bioinformatics. 2003; 19: 889–890.

756 [56] Danguy des Déserts A, Bouchet S, Sourdille P, Servin B. Evolution of recombination landscapes in
757 diverging populations of bread wheat. Genome Biol Evol. 2021; 13: evab152.

758 [57] Balfourier F, Bouchet S, Robert S, De Oliveira R, Rimbert H, Kitt J, *et al.* Worldwide phylogeography
759 and history of wheat genetic diversity. Science Advances. 2022; 5: eaav0536.

760 [58] Zhu T, Wang L, Rimbert H, Rodriguez JC, Deal KR, de Oliveira R, *et al*. Optical maps refine the bread
761 wheat *Triticum aestivum* cv. Chinese Spring genome assembly. Plant J. 2021; 107: 303–314.

762 [59] Grandaubert J, Bhattacharyya A, Stukenbrock EH. RNA-seq-based gene annotation and
763 comparative genomics of four fungal grass pathogens in the genus Zymoseptoria identify novel orphan
764 genes and species-specific invasions of transposable elements. G3 Genes Genomes Genet. 2015; 5:
765 1323–1333.

766 [60] Cabau C, Escudié F, Djari A, Guiguen Y, Bobe J, Klopp C. Compacting and correcting Trinity and
767 Oases RNA-Seq de novo assemblies. PeerJ. 2017; 5: e2988.

768 [61] Dyrløv Bendtsen J, Nielsen H, von Heijne G, Brunak S. Improved prediction of signal peptides:
769 SignalP 3.0. J Mol Biol. 2004; 340: 783–795.

770 [62] Trapnell C, Roberts A, Goff L, Pertea G, Kim D, Kelley DR, *et al*. Differential gene and transcript
771 expression analysis of RNA-seq experiments with TopHat and Cufflinks. Nat Protoc. 2012; 7: 562–578.

772 [63] Jumper J, Evans R, Pritzel A, Green T, Figurnov M, Ronneberger O, *et al*. Highly accurate protein
773 structure prediction with AlphaFold. Nature. 2021; 596: 583–589.

774 [64] Mirdita M, Schütze K, Moriwaki Y, Heo L, Ovchinnikov S, Steinegger M. ColabFold : making protein
775 folding accessible to all. Nat Methods. 2022; 19: 679–682.

776 [65] Berman HM, Westbrook J, Feng Z, Gilliland G, Bhat TN, Weissig H, *et al*. The Protein Data Bank.
777 Nucleic Acids Res. 2000; 28: 235–242.

778 [66] Holm L. Dali server: structural unification of protein families. Nucleic Acids Res. 2022; 50: W210–
779 W215.

780 [67] Burley SK, Bhikadiya C, Bi C, Bittrich S, Chen L, Crichlow GV, *et al*. RCSB Protein Data Bank: Powerful
781 new tools for exploring 3D structures of biological macromolecules for basic and applied research and
782 education in fundamental biology, biomedicine, biotechnology, bioengineering and energy sciences.
783 Nucleic Acids Res. 2021; 49: D437–D451.

784 [68] Zhang Y, Skolnick J. TM-align: A protein structure alignment algorithm based on the TM-score.
785 Nucleic Acids Res. 2005; 33: 2302–2309.

786 [69] Sehnal D, Bittrich S, Deshpande M, Svobodová R, Berka K, Bazgier V, *et al*. Mol∗ Viewer: modern
787 web app for 3D visualization and analysis of large biomolecular structures. Nucleic Acids Res. 2021; 49:
788 W431–W437.

789 [70] Zwiers L-H, de Waard MA. Efficient *Agrobacterium tumefaciens*-mediated gene disruption in the
790 phytopathogen *Mycosphaerella graminicola*. Curr Genet. 2001; 39: 388–393.

791 [71] Omrane S, Sghyer H, Audéon C, Lanen C, Duplaix C, Walker A-S, Fillinger S. Fungicide efflux and
792 the MgMFS1 transporter contribute to the multidrug resistance phenotype in *Zymoseptoria tritici* field
793 isolates. Environ Microbiol. 2015; 17: 2805–2823.

794 [72] Li L, Stoeckert Jr CJ, Roos DS. OrthoMCL: identification of ortholog groups for eukaryotic genomes.
795 Genome Res. 2003; 13: 2178–2189.

796 [73] Sievers F, Wilm A, Dineen D, Gibson TJ, Karplus K, Li W, *et al*. Fast, scalable generation of high-
797 quality protein multiple sequence alignments using Clustal Omega. Mol Syst Biol. 2011; 7: 539.

798 [74] Capella-Gutiérrez S, Silla-Martínez JM, Gabaldón T. trimAl: a tool for automated alignment
799 trimming in large-scale phylogenetic analyses. Bioinformatics. 2009; 25: 1972–1973.

800 [75] Stamatakis A. RAxML version 8: a tool for phylogenetic analysis and post-analysis of large
801 phylogenies. Bioinformatics. 2014; 30: 1312–1313.

802 [76] Letunic I, Bork P. Interactive tree of life (iTOL) v3: an online tool for the display and annotation of
803 phylogenetic and other trees. Nucleic Acids Res. 2016; 44: W242–W245.

804 [77] Hartmann FE, Sánchez-Vallet A, McDonald BA, Croll D. A fungal wheat pathogen evolved host
805 specialization by extensive chromosomal rearrangements. ISME J. 2017; 11: 1189–1204.

806 [78] Rozas J, Ferrer-Mata A, Sánchez-DelBarrio JC, Guirao-Rico S, Librado P, Ramos-Onsins SE, Sánchez-
807 Gracia A. DnaSP 6: DNA Sequence Polymorphism analysis of large data sets. Mol Biol Evol. 2017; 34:
808 3299–3302.

809 [79] Nielsen R, Yang Z. Likelihood models for detecting positively selected amino acid sites and
810 applications to the HIV-1 envelope gene. Genetics. 1998; 148: 929–936.

811 [80] Martin DP, Murrell B, Golden M, Khoosal A, Muhire B. RDP4: Detection and analysis of
812 recombination patterns in virus genomes. Virus Evol. 2015; 1.

813

## Figures captions

**Figure 1.** GWAS identifies a candidate gene controlling avirulence on the cultivar 'Soissons'. (a) Manhattan plot representing the association of multiple SNPs with PLACN on cultivar 'Soissons'. The X and Y axes indicate positions on chromosome 1 and −log10 (*p*-value) for associations, while the red line represents the Bonferroni threshold (α=0.05). (b) Top: Gene annotations (black arrows) and transposable elements (grey arrow) on the reference genome IPO323. The candidate gene is highlighted in red. Bottom: Pairwise linkage disequilibrium plot around the lead significant SNP. The association peak is associated with several polymorphisms in the gene *Zt_1_693*. (c) The difference in PLACN of isolates carrying the virulent and avirulent alleles (based on the lead SNP). Significance difference from the mean was computed using a two-sided Mann-Whitney test (****, $p<0.0001$). (d) Gene expression profile of *Zt_1_693* measured as fragments per kilobase of exon per million mapped fragments (FPKM) throughout the time course of *Z. tritici* infection on a susceptible wheat cultivar [20].

**Figure 2.** *Zt_1_693* encodes for the avirulence gene *AvrStb9* and triggers *Stb9* resistance. (a) PLACP at 26 dpi measured after inoculation with the avirulent isolate IPO09593, the virulent isolate IPO323 and IPO323 mutants expressing the avirulent allele ($IPO323_{Avrstb9}$) or the virulent allele ($IPO323_{avrstb9}$) on cultivars 'Courtot' (*Stb9*), a 'Courtot' mutant lacking *Stb9* and 'Soissons' (details on the phenotype of each mutant is provided in Fig. S5; Table S1). Statistical significance was determined using a Tukey's HSD test. (b) Genetic mapping of *Stb9* resistance gene using linkage mapping. Top panel: Linkage map and marker position in cM. Bottom panel: Logarithm of odds (LOD) score plot of the QTL analysis (Relative AUDPC for sporulation and necrosis in black and grey, respectively) possibly containing the *Stb9* locus mapped to the long arm of the chromosome 2B. The horizontal dashed line indicates a suggestive linkage threshold (LOD = 3). The position of the marker in the QTL peak is highlighted in red. (c) Manhattan plots representing association mapping results of relative AUDPC sporulation of the avirulent (top) and virulent (bottom) isolates in the bread wheat panel. Multiple SNPs in the telomeric region of chromosome 2B associated with the avirulent isolate are located in the *Stb9* genomic region.

**Figure 3.** *AvrStb9* diversity and phylogeny in the global *Z. tritici* population. (a) The top panel shows the *AvrStb9* gene structure. Middle and low panels are sliding window analyses for nucleotide diversity (π) and Tajima's D across the *AvrStb9* locus, respectively, with a window size of 200 bp and a step size of 20 bp. The plots show a reduced nucleotide diversity and a drop in Tajima's D values, likely corresponding to a selective sweep spanning the region. (b) Schematic diagram of *AvrStb9* protein sequence with an annotation of amino acid substitutions between virulent and avirulent alleles. Substitutions potentially involved in virulence are highlighted in red. SP=Signal peptide. (c) A phylogenetic tree of *AvrStb9* protein sequence generated from a global *Z. tritici* population and the reference isolate IPO323.

**Figure 4.** Phylogenetic tree of selected *AvrStb9* orthologs/paralogs belonging to five distinct classes of Ascomycota lineages. Leaf labels are color-coded according to class and represent abbreviated names of the fungal species (Table S5). *AvrStb9* is indicated with a black arrow.

**Figure 5.** Three-dimensional structure of the protein AvrStb9 predicted with the ColabFold v1.5.2: AlphaFold2. (a) An overlay of the 3D structures of the virulent avrStb9 protein (isolate IPO323 in red) and of the avirulent AvrStb9 protein (isolate IPO09593 in blue). (b) The 3D structure of the virulent avrStb9 protein with the

852 localization of the five residues potentially involved in virulence (highlighted in yellow). The (c) virulent avrStb9
853 and (d) avirulent AvrStb9 proteins with Top panel: zoom-in on the five residues in the 3D structure, and Bottom
854 panel: distances (in Å) between the five residues.

855

856 **Supporting information captions**

857

858 **Table S1.** Mean disease phenotypes measured among wild-types, mutant and chimeric strains of
859 AvrStb9 alleles..

860 **Table S2.** Summary statistics of GWA analysis on Stb9 resistance in the BW panel. Only SNPs above
861 the Bonferroni-corrected threshold are presented.

862 **Table S3.** List of the top 10 protein tertiary structures with the highest similarity to AvrStb9 protein
863 structure (from DALI webserver; accessed in january 2023).

864 **Table S4.** List of the pairwise structure alignment results.

865 **Table S5.** List of AvrStb9 selected orthologs/paralogs identified by blastp search using OrthoMCL
866 database.

867 **Table S6.** Model test and parameter estimates of diversifying selection with codeml based on the total
868 *AvrStb9* data set.

869 **Table S7.** List of primers used in this study.

870

871 **Figure S1.** Density distribution of percentage of leaf area covered by pycnidia (PLACP) in the fungal
872 population.

873 **Figure S2.** Population structure and relatedness in the fungal population used for GWAS analysis.

874 **Figure S3.** Manhattan plots of PLACN and PLACP on the wheat cultivar 'Soissons'.

875 **Figure S4.** Improved *Avrstb9* gene model using RNA-seq reads mapped to the reference genome
876 IPO323.

877 **Figure S5.** Wild-type, mutant and chimeric strains phenotype (PLACP) on cultivars carrying or not the
878 resistance gene *Stb9* and the susceptible cultivar Taichung-29.

879 **Figure S6.** Distribution of the relative AUDPC sporulating leaf area in the bread wheat population and
880 lead GWAS SNP phenotypes.

881 **Figure S7.** *AvrStb9* paralogs and their expression profile.

882 **Figure S8.** Disease scale used for the visual assessment of percent of leaf area covered by necrosis
883 (PLACN) and by pycnidia (PLACP) after inoculation of wheat leaves with the phytopathogenic fungus
884 *Zymoseptoria tritici*.

885